


SPACE WEATHER RESEARCH IN YAKUTIA

A.V. Moiseev 

*Yu.G. Shafer Institute of Cosmophysical Research
and Aeronomy SB RAS,
Yakutsk, Russia, moiseev@ikfia.ysn.ru*

A.Yu. Gololobov 

*Yu.G. Shafer Institute of Cosmophysical Research
and Aeronomy SB RAS,
Yakutsk, Russia, golart87@gmail.com*

I.B. Ievenko 

*Yu.G. Shafer Institute of Cosmophysical Research
and Aeronomy SB RAS,
Yakutsk, Russia, ievenko@ikfia.ysn.ru*

A.A. Korsakov 

*Yu.G. Shafer Institute of Cosmophysical Research
and Aeronomy SB RAS,
Yakutsk, Russia, korsakovaa@ikfia.ysn.ru*

I.S. Petukhov 

*Yu.G. Shafer Institute of Cosmophysical Research
and Aeronomy SB RAS,
Yakutsk, Russia, i_van@ikfia.ysn.ru*

S.A. Starodubtsev 

*Yu.G. Shafer Institute of Cosmophysical Research
and Aeronomy SB RAS,
Yakutsk, Russia, starodub@ikfia.ysn.ru*

Abstract. The article reports on the studies of various manifestations of space weather (SW) on Earth, conducted by SHICRA SB RAS at the network of geophysical stations located in Yakutia. It is noted that the Institute researchers study various phenomena occurring in the solar wind and Earth's magnetosphere such as magnetic clouds, Forbush effects, magnetic storms, substorms and associated subauroral glow, as well as high-latitude impulses in the dayside magnetosphere and sudden phase anomalies in the lower ionosphere. In addition to the data from the network of stations in Yakutia, data from other domestic and foreign stations, as well as direct measurements of the parameters of the interplanetary medium and magnetosphere, carried out on various spacecraft, are used to study these phenomena.

The paper also describes physical models of magnetic clouds in the solar wind, high-latitude disturbed ionosphere, and methods for short-term forecasting of SW based on cosmic ray (CR) measurements developed at SHICRA SB RAS.

Keywords: geomagnetic Pc5 pulsations, equivalent current systems, azimuthal and meridional propagation, space weather monitoring, space weather forecast, lower ionosphere, solar flare, VLF signal, sudden phase anomaly.

INTRODUCTION. SPACE WEATHER MONITORING AND FORECASTING IN RUSSIA

With the development of high technologies, space physics research has become of great importance for fundamental and applied science. Nowadays, space weather monitoring and forecast play an equally important role in the successful operation of space technology and human safety than the ordinary weather forecast. The term “space weather” (SW) refers to the state of near-Earth space (NES). In contemporary Russia, the information on the state of NES is generally provided by geophysical stations located at high latitudes of the Russian Arctic. The number of these stations is limited due to difficulties with staff, logistics, high electricity and heat tariffs in the Arctic. In addition, these stations belong to scientific organizations subordinate to different departments such as the Ministry of Education and Science of the Russian Federation and Roshydromet. As a result, SW monitoring and forecasting is carried out by a number of Russian scientific organizations (IZMIRAN, IKI RAS, SINP MSU, LPI RAS, ISTP SB RAS, IPG, AARI, SHICRA SB RAS,

IKIR FEB RAS, etc.). Despite the SW problem importance, this work has not yet been coordinated, and each organization does it independently. By contrast, SW issues are given much more attention abroad. As far back as 1995, the National Space Weather Program was created in the United States (National Space Weather Program. Strategic Plan. Office of Federal Coordinator for Meteorological Services and Supporting Research FCM-P30-1995. Washington DC. 1995); in 2001, the European ILWS (International Living with a Star) Program was launched. China keeps up with them and has also created the National Space Science Center, Chinese Academy of Science [<http://eng.sepc.ac.cn/>]. The importance of this problem is emphasized by the creation of the scientific journals “Space Weather” and “Space Weather and Space Climate”, which very quickly became highly rated. Also noteworthy are the ground-based instruments for studying SW: a developed network of geophysical stations in the Western Hemisphere compared to the Eastern one. By contrast, the SW problem is poorly addressed in present-day Russia. The number of scientific events in the country that draw attention to this problem, such as conferences on SW held by the Joint Russian-Chinese Scientific Center for SW, is very

limited. Thus, scientific organizations engaged in SW research in Russia work under such difficult conditions.

This paper describes the network of geophysical stations of the Yu.G. Shafer Institute of Cosmophysical Research and Aeronomy SB RAS in Yakutia and presents the results of SW research the Institute carries out.

1. GEOPHYSICAL NETWORK OF STATIONS IN YAKUTIA

The main experimental measurements for studying the physical picture of phenomena in the subauroral and auroral zones are carried out on the basis of the unique meridional network of SHICRA SB RAS geophysical stations in the territory of Yakutia (Figure 1). Geophysical phenomena during substorms and magnetic storms often cover a significant latitudinal and longitudinal interval. Therefore, in a number of situations only the ground-based method of recording SW manifestations can provide general information about magnetospheric processes.

The experimental base includes a network of stations in Yakutia, among which the following stationary polygons should be highlighted:

- Yakutsk EAS Array named after D.D. Krasilnikov (Oktyomtsy);
- Yakutsk cosmic ray spectrograph named after A.I. Kuzmin (Yakutsk);
- Tixie Polar Geocosmophysical Observatory (Tixie Bay);
- Complex geophysical station Zhigansk (Zhigansk);
- The Maimaga optical station named after V.M. Ignatiev (Maimaga);
- Magnetic observatory and ionospheric station Yakutsk (Yakutsk);
- Radiophysical station “Oybenkyol” (Oybenkyol).

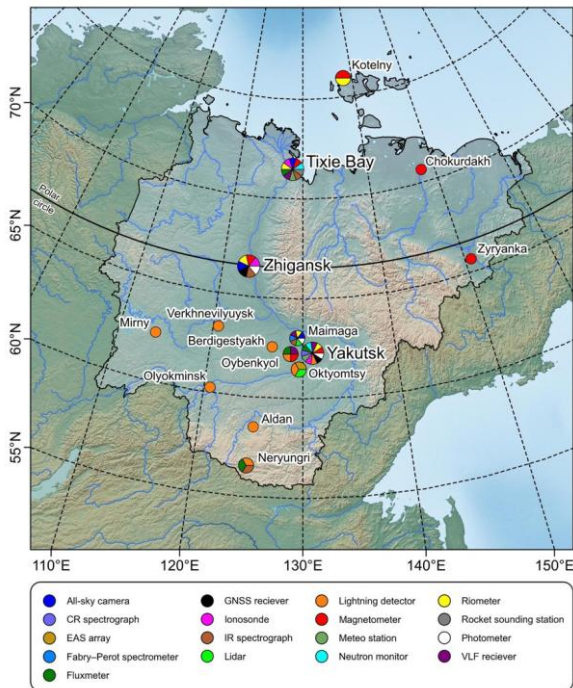


Figure 1. Stations of the meridional geophysical network in Yakutia in geographic coordinates. Measurement types are shown in color in the legend (for 2024)

According to types of spatial measurements, the following networks of stations can be distinguished in Yakutia:

- network of magnetometric stations;
- network of riometric stations;
- network of stations for measuring the atmospheric electric field intensity;
- network of stations monitoring thunderstorm activity in Yakutia.

In the area of research into the geomagnetic field and magnetospheric electromagnetic disturbances, SHICRA SB RAS participates in three large international projects — INTERMAGNET [<http://www.intermagnet.org>], MAGDAS [<http://magdas2.serc.kyushu-u.ac.jp/station/index.html>], and PWING [<http://www.isee.nagoya-u.ac.jp/dimr/PWING/en/>], and also conducts joint research with the group of low-frequency radio emissions of the Georgia Institute of Technology, Atlanta, USA. Consequently, SHICRA SB RAS stations are equipped with modern scientific instruments from the world's leading manufacturers.

2. RESULTS OF SPACE WEATHER RESEARCH AND FORECAST

Below we present the results obtained by studying SW phenomena experimentally and via modeling, as well as the result of SW forecast from satellite measurements.

2.1. Comparative analysis of meridional and azimuthal propagation of Pc5 pulsations and their current systems based on ground and satellite observations

One of the daytime impulsive high-latitude phenomena is Travelling Convection Vortices (TCVs) [Glassmeier, 1992]. TCV is a structure consisting of a pair of oppositely directed vortices in the magnetosphere, connected by field-aligned currents with vortices in the ionosphere. During its development, TCV shifts azimuthally from noon to dawn sector and along the meridian poleward. The location of magnetospheric and ionospheric TCVs, as well as the field-aligned currents connecting them in the pre-noon sector, is shown in Figure 2, *a* from [Tavares, Santiago, 1999], with arrows V_{EW} and V_{conv} indicating TCV propagation in the azimuthal direction and plasma convection respectively. According to ground-based and satellite observations, TCV consists of 2–3 pulses of opposite polarities with 5–10 min periods; TCVs are observed locally on the dayside at high latitudes. It is important to study the dynamics of TCVs in terms of SW since they cause geomagnetic field variability $|dB/dt|$ in the absence of magnetic storms and can affect technical infrastructure at high latitudes [Pili-penko et al., 2023].

Moiseev et al. [2024a] have used ground observations in 8 events to compare TCV velocities by phase delays of Pc5 pulsations and by the motion of their equivalent current systems. Figure 2, *b*, *c* presents histograms of meridional velocities; and Figure 2, *d*, *e*, of azimuthal velocities. On the ordinate axis in Figure 2, *b*, *d* is the number of measurements of Pc5 pulsation velocities

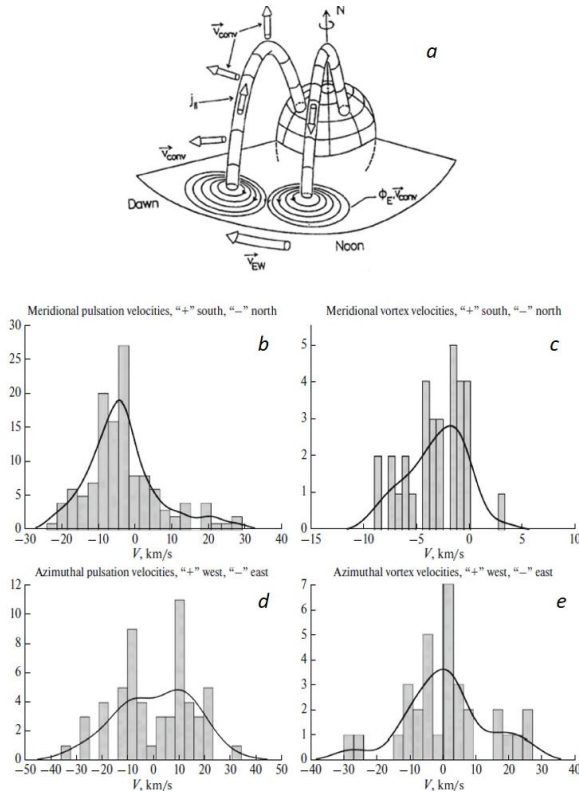


Figure 2. Travelling convection vortices in the magnetosphere and ionosphere (a); histograms of propagation velocities of geomagnetic pulsations and equivalent current vortices; meridional velocities (b, c); azimuthal velocities (d, e)

on the ordinate axis in Figure 2, c, e is the number of measurements of vortex propagation velocities. The histograms show a smoothing line as the result of a nonparametric method for estimating the density of random variable (Kernel Density Estimation). It is evident from the histograms that propagation of pulsations and vortices is similar: along the meridian, pulsations and vortices predominantly propagate to the north. In most cases, propagation velocities of pulsations and vortices were ~ 5 km/s and 2 km/s respectively, whereas in azimuth, pulsations and vortices propagate to the west, their propagation velocities were ~ 10 km/s and 3 km/s respectively. However, in the distribution of azimuthal velocities of both pulsations and vortices there are comparable maxima corresponding to eastward propagation: the velocity of pulsations is 10 km/s, and that of vortices is 5 km/s. Moiseev et al. [2024b] have studied TCV propagation, using satellite and ground-based observations. Pulsations in the magnetosphere and ionosphere, and equivalent current vortices in the ionosphere were found to propagate in the azimuthal direction from the day side to the night side. The propagation velocities according to ground observations are 5–25 km/s; according to satellite observations, 114–236 km/s.

The results of the work show that the dynamics of equivalent current systems correspond to the dynamics of pulsations, and they can be utilized to study propagation as an additional method, especially when it is impossible to determine propagation velocities from phase delays, but it is necessary to take into account the difference between velocities of pulsations and vortices.

TCVs are recorded in an extended longitude sector (up to 12 hours). It is assumed that the observed dynamics of Pc5 pulsations and vortices reflects propagation of MHD waves in the magnetosphere, not only from the day side to the night side, but also in the opposite direction (from the night side to the noon side).

2.2. Study of the magnitude of sudden phase anomalies on VLF radio paths during solar flares

Changes in lower ionosphere parameters are sensitive to space weather events [Silber, Price, 2017]. Very low frequency (VLF 3–30 kHz) radio waves propagate for a long distance as in a waveguide due to reflection from water, ground, and lower ionosphere. An increase in the X-ray flux intensity during solar flares leads to sudden ionospheric disturbances (SIDs). A sharp increase in the electron density during SIDs causes sudden phase anomalies (SPAs) of VLF radio signals during daytime propagation in the Earth — ionosphere waveguide [Kumar, Kumar, 2018]. Recording of VLF signal parameters allows ionosphere research to be conducted with high resolution both in time and space. The Antarctic-Arctic Radiation-belt (Dynamic) Deposition-VLF Atmospheric Research Consortium is widely known, it provides continuous observations of the lower ionosphere in the polar regions [Clilverd et al., 2009]. The problem of high-resolution VLF monitoring of large, hard-to-reach areas of the Pacific Ocean and Northern Asia remains unresolved [Wendt et al., 2024]. VLF observations in Yakutia are described below.

In Yakutsk (62.02° N, 129.70° E) and in the Polar Geocosmophysical Observatory (PGO) in Tixie Bay (71.60° N, 128.90° E), SHICRA SB RAS records signals from VLF radio transmitters. The phase variations of signals from the transmitters Khabarovsk (Russia, RSDN-20 system, 50.07° N, 136.6° E, signal frequency 11.904 kHz) and NWC (Australia, 21.82° S, 114.17° E, signal frequency 19.8 kHz) have been selected for the analysis [Kozlov et al., 2025]. Radio propagation paths Khabarovsk—Yakutsk (the length is 1.4 Mm) and NWC—Yakutsk (the length is 9.4 Mm) cover the East Asia territory. SPAs of signals from the Khabarovsk and NWC transmitters recorded in Yakutsk are plotted in Figure 3 as a function of solar X-ray flux. Changes in the VLF signal phase Φ relative to the undisturbed value are reduced to the propagation path length unit (deg/Mm). The value P is the maximum X-ray flux intensity (0.1–0.8 nm) during a solar flare (W/m^2). The value $\cos X$ is the cosine of a solar zenith angle X averaged along the entire propagation path. The solar zenith angle X was calculated from geographic coordinates along each of the radio paths with a step of 200 km by the algorithm [<http://stjarnhimlen.se/comp/tutorial.html>].

The standard deviations of residuals are 1.37 deg/Mm (the Khabarovsk—Yakutsk propagation path) and 1.73 deg/Mm (the NWC—Yakutsk propagation path). The reliability level of model SPA parameters is not lower than 98 % (the Fisher criterion). The SPA model parameters were applied to solar flares for the VLF propagation paths. The X-ray flux during solar flares can be estimated by the ground-based method, using VLF data [George et al., 2019; Korsakov et al., 2021].

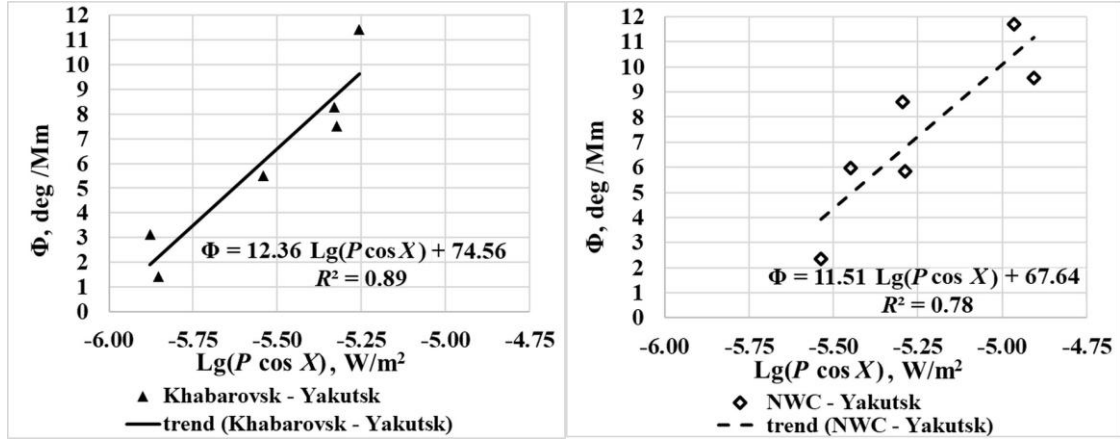


Figure 3. Sudden phase anomalies Φ of signals from transmitters Khabarovsk (left) and NWC (right) recorded in Yakutsk as a function of solar X-ray flux

2.3. Relationship of the SAR arc to the energetic ion flux boundary inside the plasmasphere and the plasmopause based on ground and satellite observations

Stable auroral red (SAR) arcs occur during magnetic storms due to overlap of the ring current with the outer plasmasphere, where energetic ion fluxes heat plasmaspheric electrons. SAR arcs are optical manifestations of SW in Earth's atmosphere. The resulting downward flux of superthermal electrons along magnetic field lines increases the ambient electron temperature at altitudes of the ionospheric F2 region in the form of a subauroral electron temperature peak (T_e peak). As a result, the intensity of the red line of atomic oxygen in the SAR arc, which reflects the plasmopause, increases [Cole, 1965, 1970; Cornwall et al., 1971; Kozyra et al., 1997]. Long-term observations of subauroral glow at the Yakutsk meridian have shown that under conditions of low magnetic activity ($Dst \geq -50$ nT, $K_p \leq 3-4$) SAR arcs appear during individual substorms and are observed at corrected geomagnetic latitudes (CGMLat) $55-60^\circ$ [Ievenko, 1999; Ievenko, Alekseev, 2004]. During periods of high geomagnetic activity, SAR arcs are recorded at lower latitudes.

Below are the results of comparison of SAR arc observations by the digital all-sky camera (All-sky imager "Keo Sentry") at the station Maimaga (CGMLat= 58° , CGMLon= 202°) with data from simultaneous recording of plasmopause and energetic ion fluxes on board the Van Allen Probe B (VAP-B) satellite at the beginning of the major magnetic storm on March 17, 2015 [Ievenko, 2020; Ievenko, Parnikov, 2020].

The ground-based and satellite observations in Figure 4 show the following.

1. An intense SAR arc was observed equatorward of the diffuse aurorae at low auroral activity at CGMLat= $52-59^\circ$ in the dusk MLT sector. Variations in the intensity and location of the red arc during the period considered were insignificant (a).

2. At 12:10:10 UT ($\sim 18:52$ MLT), the equatorial edge of the red arc at CGMLon $\sim 179^\circ$ coincided with the boundary of the flux of energetic H^+ and O^+ ions

inside the plasmasphere at $L \sim 2.8$, as measured by VAP-B at $\sim 17:36$ MLT (b).

3. At 12:45:10 UT ($\sim 19:05$ MLT), the polar edge of the arc at CGMLon $\sim 174^\circ$ was due to a sharp decrease in the electron density to $\sim 100 \text{ cm}^{-3}$ (plasmopause) at $L \sim 4.0$ at $\sim 19:05$ MLT (b).

4. The width and location of the SAR arc were in good agreement with the intense T_e peak, as measured by DMSP-19 in the dusk MLT sector at $\sim 11:54$ UT (c). Electron temperature measurements verify ground-based observations of the SAR arc.

2.4. Study of ionospheric disturbances based on numerical modeling of large-scale structure of the ionosphere

The high-latitude ionosphere has a complex structure and is characterized by the presence of regular large-scale structural features such as the tongue of ionization and polar cavity at high latitudes, polar and auroral peaks in the daytime cusp region and in the night sector, as well as the main ionospheric trough (MIT) at subauroral latitudes [Mizun, 1980]. The ionosphere depends significantly on SW. Thus, during geomagnetic storms, the configurations of these structural features become more complex, which is mainly caused by the disturbance of the large-scale electric field of magnetospheric convection controlled by the orientation of the interplanetary magnetic field (IMF). Changes in the electron density distribution in turn affect radio wave propagation and the positioning accuracy of global navigation satellite systems (GNSS).

SHICRA SB RAS conducts research into the large-scale structure of the ionosphere and the processes occurring in it, using the developed non-stationary three-dimensional model of the ionosphere in Euler variables [Kolesnik, Golikov, 1982; Golikov et al., 2005, 2012, 2016]. Below are the results of the study into the effect of magnetospheric convection on the large-scale structure of the ionosphere during a moderate geomagnetic storm for winter conditions ($\delta = -23^\circ$). Two diametrically opposed scenarios are considered: 1) with the onset of the storm at 16 UT; 2) with the onset of the storm at 04 UT.

Figure 5 illustrates variations in the IMF B_z component (a) and geomagnetic activity indices Dst and AL (b) and spatiotemporal distributions of the electron density at the F2 maximum altitude (n_mF2) at different moments of universal time (UT) at the onset of the storm at 16 UT (c–e) and 04 UT (f–h). Under quiet conditions (Figure 5, c), the convection region is seen to partially enter the illuminated zone above the terminator at 16 UT, which leads to transfer of plasma from the dayside ionosphere to the night side and the formation of an ionization tongue. In polar latitudes ($\Phi_m \geq 80^\circ$), a region of low n_mF2 is formed — a polar cavity surrounded by ionization in the auroral oval (Figure 5, c). In the latitudinal variation in the dusk sector in the full

shadow region [Kolesnik, Golikov, 1982], a deep concentration trough is observed: the main ionospheric trough (MIT) (Figure 5, c). After the onset of the disturbance, convection intensifies and its area of action increases (Figure 5, d, e). This causes an increase in the area of overlap of the convection region with the illuminated ionosphere and hence an increase in the transfer of dayside ionization to the night side by the anti-sunward flow, subsequent extension of the ionization tongue in the day-night direction, and the disappearance of the polar cavity at 19 UT. At 22 UT, the depth of MIT decreases, and MIT shifts southward by $\sim 5^\circ$ – 10° .

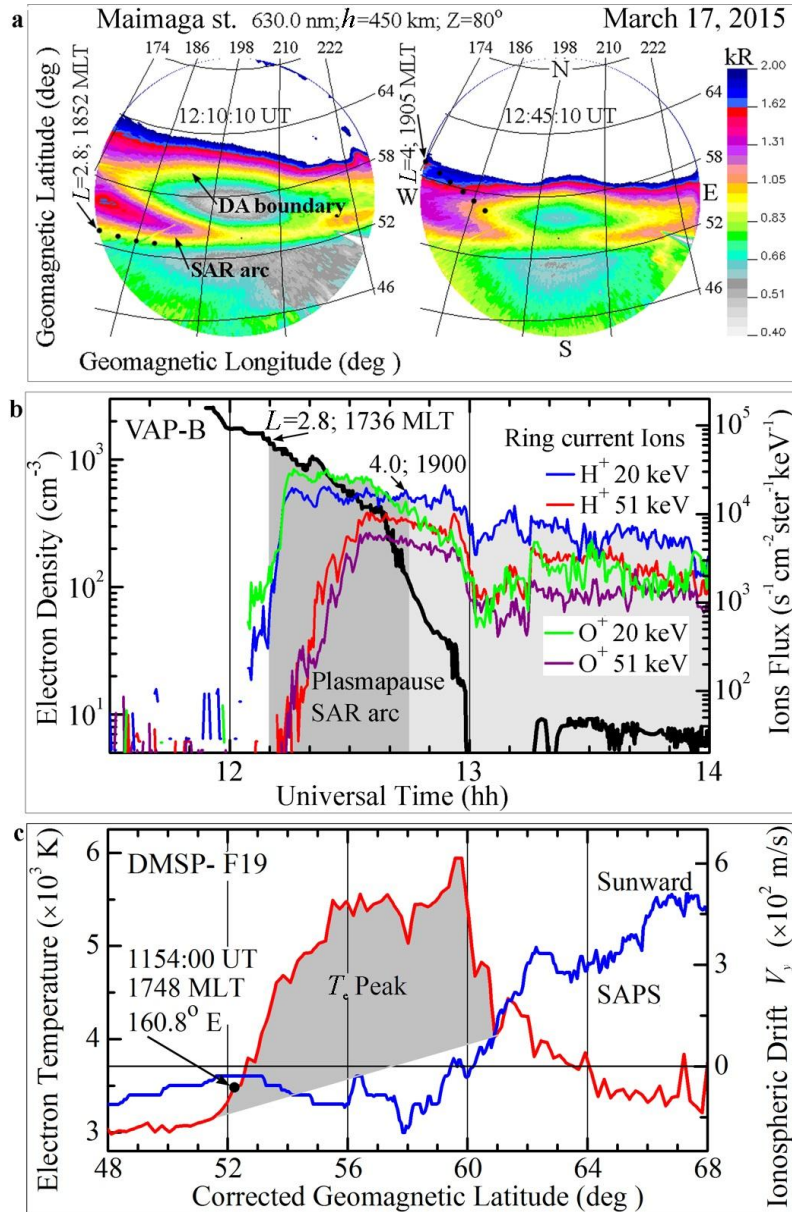


Figure 4. SAR arc at Maimaga station during recording of plasmopause energetic ion fluxes and T_e peak on board the VAP-B and DMSP-F19 satellites, respectively, on March 17, 2015. All sky images in the 630.0 nm emission projected onto Earth's surface for the glow altitude of 450 km ($Z \leq 80^\circ$) in corrected geomagnetic coordinates (a). The color scale of the emission intensity is given only up to two kilorayleigh (kR) for better display of the SAR arc. The density of thermal electrons and fluxes of energetic protons and oxygen ions (b). The dark gray column shows the region of VAP-B measurements, which was conjugate with the observed SAR arc. Latitudinal distribution (c) of electron temperature and ionospheric drift in the F region based on DMSP-F19 measurements in the dusk MLT sector. The bold dot marks the location of the equatorial boundary of the T_e peak, with magnetic longitude and MLT indicated

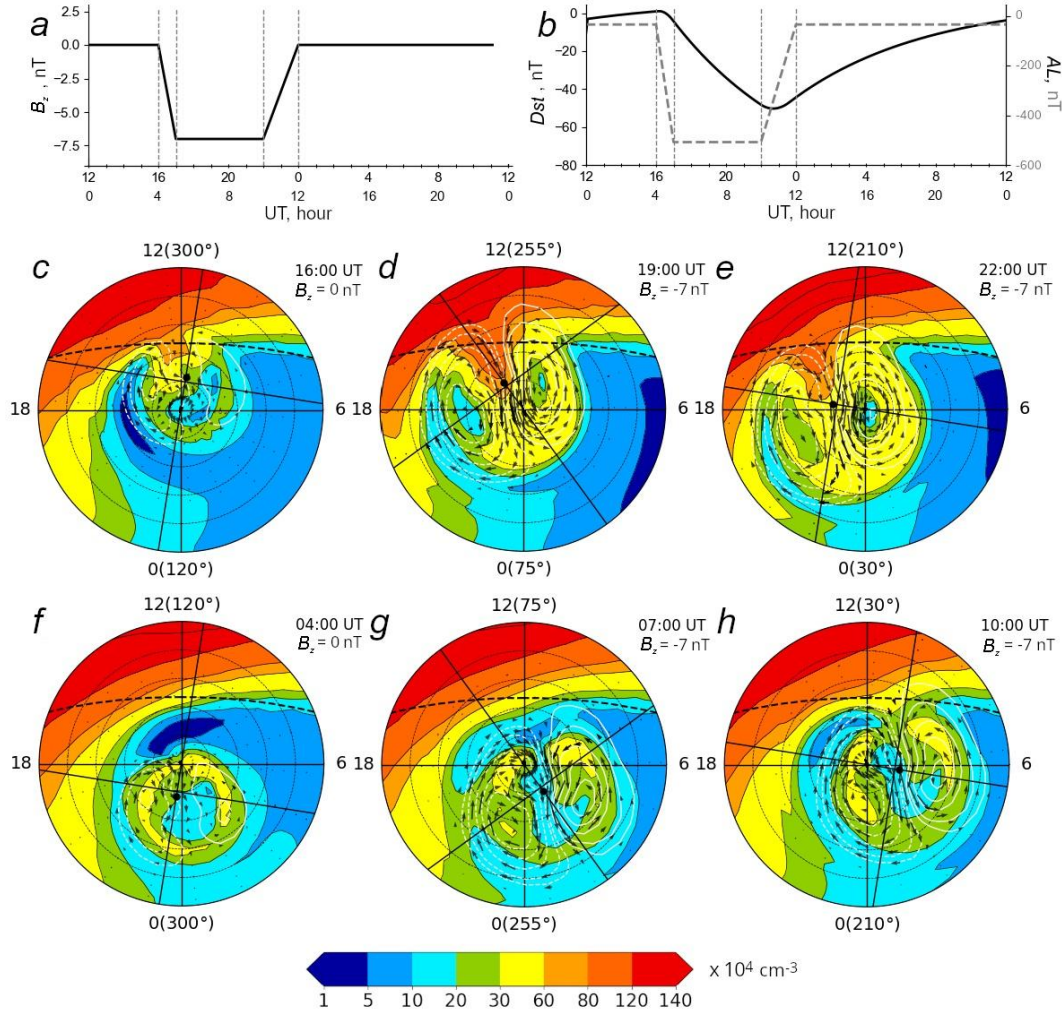


Figure 5. IMF B_z component (a), geomagnetic activity indices Dst and AL (b), and spatiotemporal distributions of the electron density at the height of the F2 maximum ($n_m F2$) at different moments of universal time at the onset of the storm at 16 UT (c–e) and 04 UT (f–h). Concentric circles denote the geographic latitudes of the Northern Hemisphere drawn through 10°. The lower boundary corresponds to 40° N. The numbers near the outer circle are local time and next to them in brackets are geographic longitude. The dashed line (upper) is the position of the terminator at the zenith angle $\chi = 90^\circ$. The intersection point of two mutually perpendicular lines is the geomagnetic pole, which is 11.5° away from the geographic pole. The arrows indicate drift velocities of ionospheric plasma caused by the electric field of magnetospheric convection. White isolines show the electric field potentials calculated by the Weimer model [Weimer, 1996]. Charged particle precipitation is specified using the APM PGIA model [Vorobjev et al., 2013]

The storm onset at 04 UT is diametrically opposite to the magnetic storm onset at 16 UT (Figure 5, f–h). In this case, the Eastern Hemisphere is on the day side. As can be seen, at 04 UT the geomagnetic pole and with it the convection and precipitation region are located entirely on the night side (Figure 5, f). As a result, the ionization tongue is seen to separate from the dayside ionosphere. In the latitudinal variation on the dayside in the range 70–80° N, a great dip in $n_m F2$ is observed — a daytime dip (Figure 5, f) [Kolesnik, Golikov, 1984]. At CGMLat above ~80°, a polar cavity is formed, where $n_m F2 \leq 10^4 \text{ cm}^{-3}$. After the disturbance starts, the increase in magnetospheric convection leads to the expansion of the detached tongue of ionization and to the smoothing of the auroral peaks of $n_m F2$ (Figure 5, g, h). At 07 UT, convection covers the daytime trough and significantly increases $n_m F2$ compared to their values under quiet conditions (Figure 5, g, f).

Thus, magnetospheric convection during a moderate magnetic storm causes a change in the shapes and sizes of the main large-scale structural features of the ionosphere and depends on the time of the geomagnetic storm onset due to the displacement of the geographic and geomagnetic poles. The storm effect is most pronounced in the case of storm onset at 16 UT, when the disturbed electric field of magnetospheric convection enhances the transfer of plasma from the dayside ionosphere to the night side. The results are presented in more detail in [Gololobov, Golikov, 2024; Gololobov et al., 2025].

2.5. Explanation of Forbush decreases in cosmic rays based on a physical model

Large-scale coronal mass ejections (CMEs) are one of the largest energetic events on the Sun and an important factor in SW affecting geomagnetic activity, the

spatiotemporal distribution of CRs, and solar wind plasma properties. The modern approach to determining the properties of ejections and their identification in interplanetary space is usually based on the use of local spacecraft measurements. Since the number and spatial coverage of such spacecraft are fairly limited, there is a need for alternative sources of information, for example, CR measurements, which, due to high mobility, contain information about large-scale properties of the medium.

Part of CME is magnetic clouds (MCs) — areas filled with a helical magnetic field. Due to its force-free structure, such a field is preserved at large distances. Some MCs are oriented in such a way that in the vicinity of Earth, regular IMF will have a high intensity and a long-term southern orientation, which is a necessary condition for the occurrence of a geomagnetic storm.

To determine properties of MC from observed characteristics of CRs, it is necessary to describe their interaction. We have proposed an electromagnetic mechanism for such interaction. In this mechanism, particle scattering is neglected, and propagation is determined only by the magnetic field of the ejection and the electric field induced in the moving plasma. By calculating trajectories of CRs from the point of interest to the source (the point where the characteristics have not yet been altered by the Sun), it is possible to determine the change in their energy and the corresponding change in intensity. For theoretical calculations, an MC model has also been proposed which allows us to identify the magnetic field at an arbitrary point at any time.

The calculations have shown that the energy losses during the motion of CRs in the induced electric field, although small, are monotonous; hence, the longer the particle moves in interplanetary space, the more energy it loses, which leads to a decrease in the recorded intensity of CRs (Figure 6, *a*).

Since the calculations allow us to determine the CR distribution function, knowing it, we can find not only the zero moment (the integral intensity), but also higher moments: the first — the vector anisotropy (Figure 6, *b*), and the second — the tensor anisotropy (Figure 6, *c*, *d*). The CR anisotropy inside MC increases, which is consistent with experimental observations. Comparison of the experimental results with calculations suggests that the adopted assumptions and the constructed models are adequate. The method and the results obtained on its basis are described in more detail in [Petukhova et al., 2019, 2020].

In the future, it is planned to take into account in the model not only the magnetic field of MC, but also the effect of the coronal mass ejection plasma, the region of compressed solar wind, and the shock wave on CRs. This will allow a more accurate determination of ejection properties long before it arrives at Earth's orbit and hence refinement of space weather forecast.

2.6. Forecast of geoeffective disturbances from satellite and ground cosmic ray measurements

Since 2009, SHICRA SB RAS has been conducting an experiment on short-term (1–2 days) forecasting of the arrival of large-scale SW disturbances into the Earth

orbit, such as interplanetary shock waves (ISWs) and high-speed SW streams, using measurements from the global network of CR stations, which include SHICRA SB RAS stations Yakutsk and Tixie Bay, as well as real-time spacecraft (SC) measurements of interplanetary medium parameters.

In this paper, we illustrate the capabilities of the ISW forecast from 1 hr [<ftp://ftp.swpc.noaa.gov/pub/lists/ace2/>] and 1 min ACE SC data [<ftp://ftp.swpc.noaa.gov/pub/lists/ace/>]. This SC is located near the libration point L1 at a distance of ~1500000 km from Earth toward the Sun. The flight time of large-scale SW disturbances from the location of ACE SC to Earth's magnetosphere is on average ~1 hr, which is clearly insufficient for taking any preventive measures to prevent possible negative effects of SW changes on various technical space or ground systems. However, the forecast method we developed using data from this SC allows us to receive a warning about upcoming changes in SW much longer in advance, ~1 day.

Of all the experiments conducted on board ACE SC, we use data from the MAG, SWEPAM, and EPAM experiments. In the latter case, the data is from measurements of proton fluxes in 8 different differential energy channels with energies from 47 to 4800 keV, which are measured by the LEMS120 detector. Note that all data is primary and so should be analyzed with a certain caution, and possible risks associated with their use must be assumed.

At present, we have already accumulated the necessary knowledge to construct a physical picture of the occurrence of fluctuations (or short-term variations with periods less than 3 hrs) of CR in order to apply it to a forecast of the arrival of large-scale solar wind disturbances at the Earth orbit [Berezhko, Starodubtsev, 1988; Starodubtsev et al., 1996; Grigoryev et al., 2008]. In brief, the knowledge boils down to the following.

In many cases, significant CR fluxes with ~1 MeV energies are often observed in the region before large-scale solar wind disturbances, e.g. ISWs or high-speed solar wind streams. Moreover, compared to the background, these CRs are characterized by large values of both the fluxes and their gradients. This leads to the development of plasma instabilities, which in turn are converted into MHD waves of various types. If fast magnetosonic waves develop in interplanetary space before the aforementioned solar wind disturbances, they, in turn, modulate the isotropic part of the CR distribution function in a wide energy range (from tens of keV to units of GeV) and hence lead to the emergence of CR fluctuations. Nonetheless, since CR fluctuations have a low amplitude (less than 1 %), then to isolate them against the background of the persistent noise, it is necessary to correctly apply spectral analysis methods [Starodubtsev et al., 2023]. One of the methods for forecasting SW developed at SHICRA SB RAS from CR measurements is based on these concepts.

The fluctuation extraction technique involves calculating the coherence between CR flux measurements in different differential channels in the EPAM/LEMS120 experiment. According to the results obtained in [Grigo-

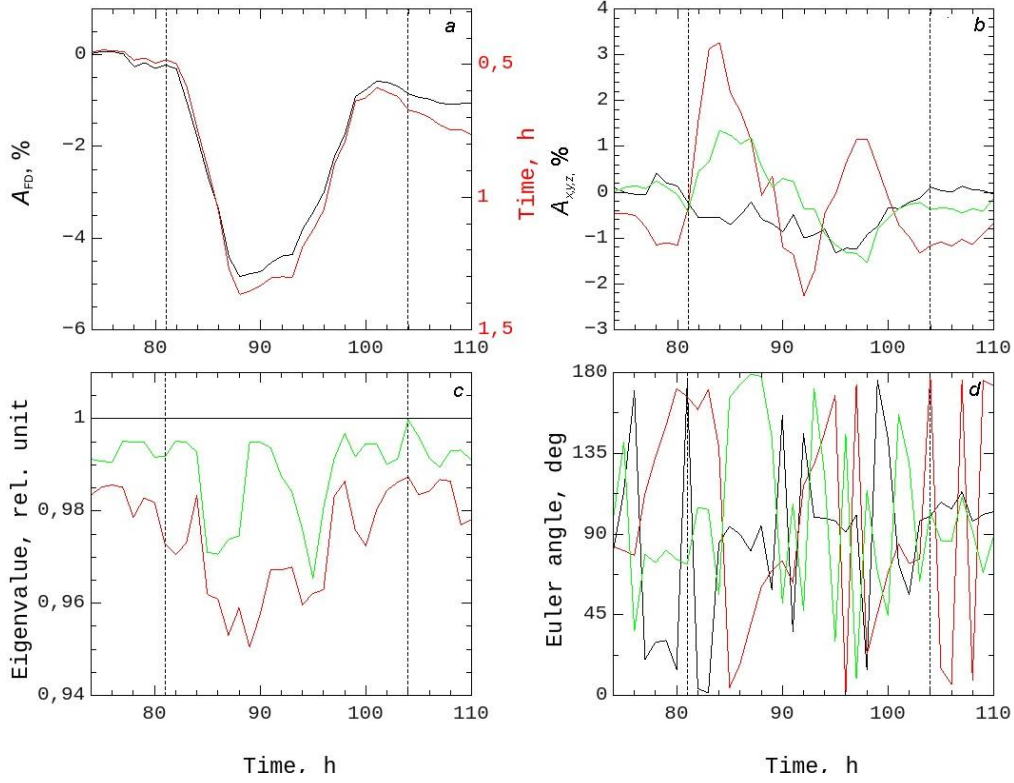


Figure 6. Characteristics of the Forbush decrease in time: *a* — the amplitude of the Forbush decrease is shown by the black curve (left scale); and the average time of CR transition from the surrounding space to MC, by the red curve (right scale); *b* — vector anisotropy component (black curve — A_x ; red curve — A_y ; green curve — A_z); *c* — relative eigenvalues (the maximum eigenvalue, indicated by the black line, is 1; green curve is the average; red curve is the smallest); *d* — three Euler angles defining the orientation of the ellipsoid (black and red curves are α_1 , α_2 ; green curve, α_3). $B_m = 11.6$ nT is maximum magnetic field strength when MC crosses Earth. Dashed vertical lines are the leading and trailing boundaries of MC

ryev et al., 2008], there is a significant CR coherence value between CRs with different energies in the frequency range above 10^{-4} Hz in the case of significant CR fluxes in the region of the ISW pre-front. Our experience shows that for forecasting purposes it is necessary for the coherence to exceed a certain critical level equal to 0.85, and it is sufficient for this to occur not in the entire range, but at individual frequencies that correspond to the inertial section of the MHD wave turbulence spectrum, where fast magnetosonic waves are observed. Therefore, as a precursor of the arrival of interplanetary disturbances of the solar wind at the Earth orbit we utilize a maximum coherence coefficient (Coh MAX) between measurements in the energy channels P2 and P5. As an example, let us consider the ISW event of May 10, 2024. Figure 7, *a–e* presents 1-hr measurement data on the IMF modulus and B_z component (*a*), solar wind density (*b*), temperature (*c*), and velocity (*d*), as well as Dst (*e*) for the event under study from May 8 to 13, 2024. It is evident that at the leading edge of strong ISW at $\sim 18:00$ UT on May 10, 2024, all parameters significantly exceeded their average values. In this case, the IMF modulus B was more than 40 nT, the B_z component was less than -16 nT, the solar wind plasma density $n \approx 33 \text{ cm}^{-3}$, its temperature $T \approx 5 \cdot 10^5 \text{ K}$, and the solar wind speed U was as high as 680 km/s (Figure 7, *a–d*). Since this was a complex event in all respects, caused by almost simultaneous arrival of multiple CMEs at Earth [Hayakawa et al., 2025; Lazzús, Salfate,

2024; Ram et al., 2024], all SW parameters subsequently changed even more dramatically. The passage of this

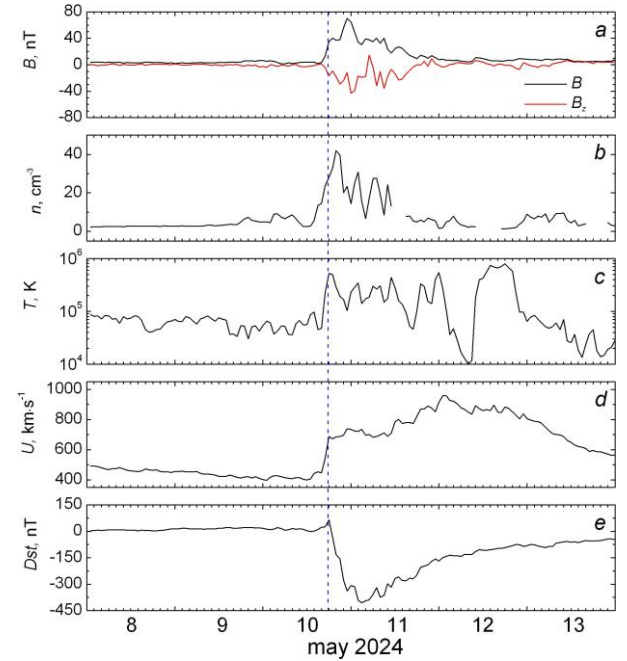


Figure 7. Variations in the IMF modulus B and B_z component (*a*), density n (*b*), temperature T (*c*) and solar wind velocity U (*d*), as well as the Dst index (*e*) for May 8–13, 2024, as measured by ACE SC. The vertical dashed line indicates the arrival of ISW at ACE SC and the storm sudden commencement (SSC)

strong ISW caused a powerful geomagnetic storm with SSC (Figure 7, e). This storm began at 17:05 UT on May 10, 2024. As a result of the passage of multiple CMEs through the Earth orbit, Dst at the storm minimum decreased to -406 nT [https://omniweb.gsfc.nasa.gov/ow.html]. It was the most powerful geomagnetic storm observed in the last two decades since the famous event of November 20, 2003, which is known in the scientific literature as the Halloween Event [Piersanti et al., 2025].

Figure 8 presents the results of the ISW arrival forecast and it needs some explanations. The names of the experiments and the corresponding SC on board which they are conducted are given at the top of the figure. Further, from top to bottom, the large panels show the time dependence of the variations in the IMF modulus B and B_z component, the SW plasma velocity U and density n , the low-energy CR flux J , and the maximum value of the coherence coefficient between measurements in the P2 and P5 energy channels (Cohar MAX). Vertical lines designate the universal time (UT), which is given

under the bottom panel as day of the year. Four bottom small panels from left to right exhibit the current values of the IMF power spectrum density and the power function approximating it, as well as the coherence coefficients depending on the frequency between B and U , B and n , and between P2 and P5. Note that the coherence values between B and U reflect the contribution of Alfvén waves to the observed power spectrum of IMF; B and n , that of fast magnetosonic waves. Inscriptions below these panels contain information about the fact of using data in real time and the time of creating the figure. In the case of generating a forecast, a red inscription appears in Figure 8, which states that an interplanetary disturbance is expected to arrive at the spacecraft within ~ 1 day.

It is evident from Figure 8 that, as expected, increased low-energy CR fluxes were observed in this event in the region of the strong ISW pre-front. It can therefore be expected that they will generate fast magnetosonic waves in the region of the ISW pre-front, which will modulate the isotropic part of the CR flux and

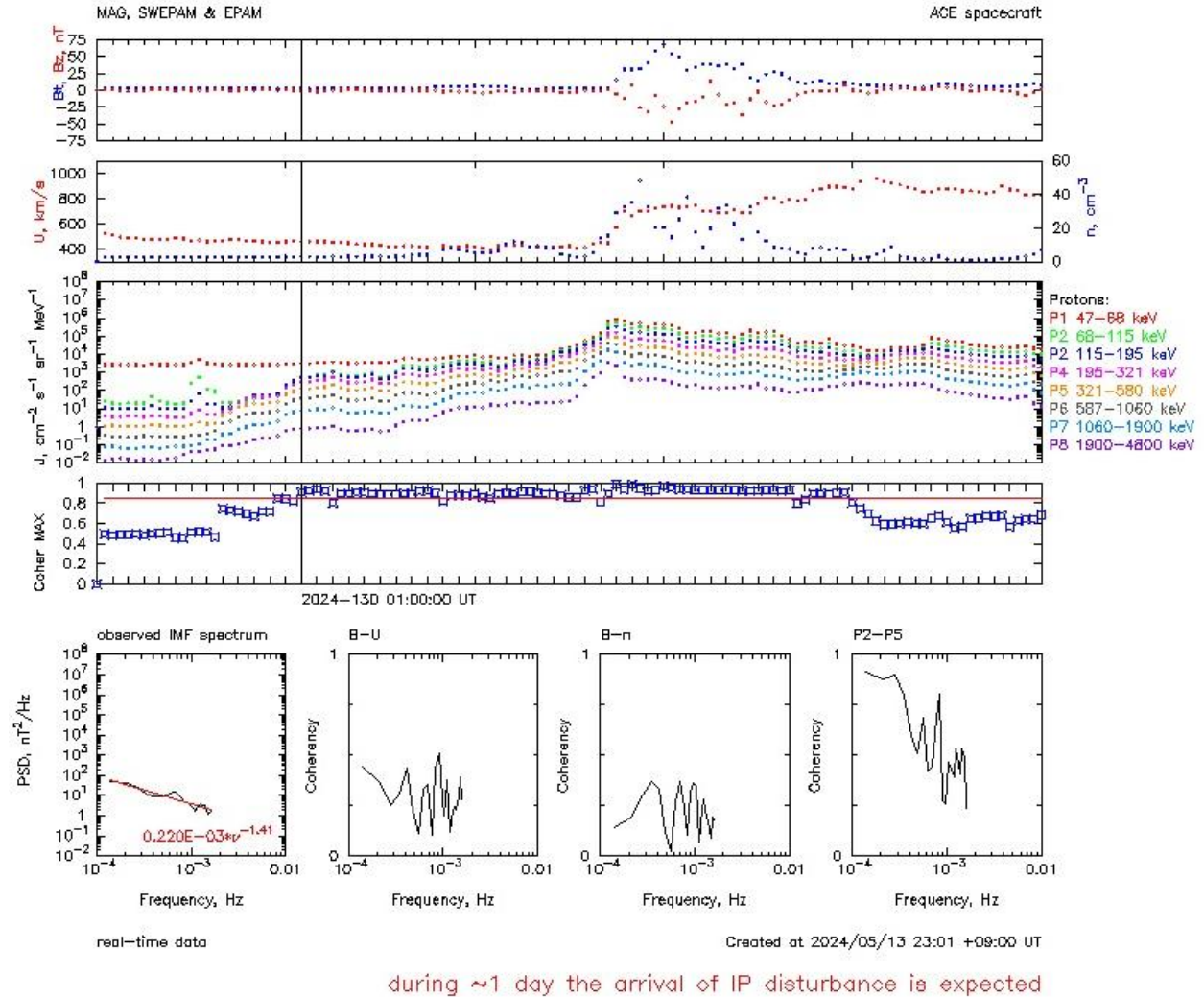


Figure 8. Variations in the IMF modulus B and the B_z component (top panel), the solar wind plasma velocity U and density n (second panel from the top), the low-energy CR flux J (third panel from the top), the maximum value of the coherence coefficient between measurements of the J energy channels P2 and P5 (fourth panel from the top), the red horizontal line indicates the critical level depending on time. The vertical lines show the current time. A legend is given for the differential CR energy channels. Four bottom panels from left to right present the current values: the density of the IMF power spectrum and the power function approximating it; the coherence coefficients between B and U , B and n , and between P4 and P5

lead to the occurrence of fluctuations a sufficiently long time before the arrival of ISW. Indeed, the first maximum values of coherence between the channels of recording of proton fluxes P2 and P5 with energies 115–195 and 1060–1900 keV respectively, exceeding the critical level were observed at 01:00 UT on May 9, 2024, 36 hours before the arrival of ISW at ACE SC and remained above this level until 22:00 UT on May 11, i.e. until the SW parameters were disturbed (see Figure 8).

Thus, based on ACE SC measurements of CR fluxes with a lead time of 36 hours, a forecast was given for the arrival of a large-scale SW disturbance of the ISW type at the Earth orbit on May 10, 2024. Our experience shows that in such cases the accuracy of the forecast is ~80 %.

Note also that SHICRA SB RAS has been continuously monitoring near-Earth space in real time for many years. For this purpose, measurement data is employed from ACE SC and on the CR intensity from the stations Yakutsk and Tixie Bay. All calculations are performed automatically once per hour, using the *cron* daemon program under the control of the Linux operating system. All output information, including measurement data and calculation results in graphical form, is available at [<https://www.ysn.ru/~starodub/CosmicRayFluctuations/index.html>].

CONCLUSION

The SW phenomena of different spatial scales have been studied: global (magnetic storm), local (TCV, substorm). Local phenomena are recorded in the daytime (TCV) and nighttime sectors (substorm). We have examined the formation of disturbances in the solar wind and their development in the magnetosphere. Using the example of a strong magnetic storm in May 2024, the result of a short-term forecast of the arrival of a large-scale solar wind disturbance of the ISW type at the Earth orbit with a lead time of 36 hours has been shown.

SHICRA SB RAS is ready to participate in international projects, as well as in collaborations with Russian scientific organizations in the field of space weather.

The work was financially supported by the Ministry of Science and Higher Education of the Russian Federation.

REFERENCES

- Berezhko E.G., Starodubtsev S.A. Nature of the dynamics of the cosmic-ray fluctuation spectrum. *Bull. Academy of Sciences of USSR. Ser. Physics*. 1988, vol. 52, pp. 2361–2363.
- Clilverd M.A., Rodger C.J., Thomson N.R., Brundell J.B., Ulich T., Lichtenberger J., Cobbett N., et al. Remote sensing space weather events: Antarctic-Arctic radiation-belt (dynamic) deposition-VLF atmospheric research Consortium network. *Space Weather*. 2009, vol. 7, iss. 4, S04001. DOI: [10.1029/2008SW000412](https://doi.org/10.1029/2008SW000412).
- Cole K.D. Stable auroral red arcs, sinks for energy of *Dst* main phase. *J. Geophys. Res.* 1965, vol. 70, iss. 7, pp. 1689–1706.
- Cole K.D. Magnetospheric processes leading to mid-latitude auroras. *Ann. Geophys.* 1970, vol. 26, iss. 1, pp. 187–193.
- Cornwall J.M., Coroniti F.V., Thorne R.M. Unified theory of SAR arc formation at the plasmopause. *J. Geophys. Res.* 1971, vol. 76, iss. 19, pp. 4428–4445.
- George H.E., Rodger C.J., Clilverd M.A., Cresswell-Moorcock K., Brundell J.B., Thomson N.R. Developing a nowcasting capability for X-Class solar flares using VLF radiowave propagation changes. *Space Weather*. 2019, vol. 17, iss. 12, pp. 1783–1799. DOI: [10.1029/2019SW002297](https://doi.org/10.1029/2019SW002297).
- Glassmeier K.-H. Traveling magnetospheric convection twin vortices: Observations and theory. *Ann. Geophys.* 1992, vol. 10, iss. 8, pp. 547–565.
- Golikov I.A., Kolesnik A.G., Chernyshov V.I., Popov V.I. Mathematical model of the F2 region of the high-latitude ionosphere taking into account the thermal regime. *Bull. Yakutsk State University*, 2005, vol. 2, iss. 3, pp. 61–69.
- Golikov I.A., Gololobov A.Yu., Popov V.I. Numerical modeling of the thermal regime of the high-latitude ionosphere. *Bull. North-Eastern Federal University*, 2012, vol. 9, iss. 3, pp. 22–28.
- Golikov I.A., Gololobov A.Yu., Popov V.I. Modeling the electron temperature distribution in F2 region of high-latitude ionosphere for winter solstice conditions. *Sol.-Terr. Phys.* 2016, vol. 2, iss. 4, pp. 54–61. DOI: [10.12737/19424](https://doi.org/10.12737/19424).
- Gololobov A.Yu., Golikov I.A. Numerical modeling of the influence of IMF on the large-scale structure of the ionosphere taking into account the misalignment of the poles. *Bull. North-Eastern Federal University*. 2024, vol. 21, iss. 1, pp. 45–57. DOI: [10.25587/2222-5404-2024-21-1-45-57](https://doi.org/10.25587/2222-5404-2024-21-1-45-57).
- Gololobov A.Yu., Golikov I.A., Popov V.I. Modeling of the influence of magnetospheric storm on the large-scale structure of the high-latitude ionosphere for winter solstice conditions. *Sol.-Terr. Phys.* 2025, vol. 11, iss. 2, pp. 88–98. DOI: [10.12737/stp-112202509](https://doi.org/10.12737/stp-112202509).
- Grigoryev A.V., Starodubtsev S.A., Grigoryev V.G., Usoskin I.G., Mursula K. Fluctuations of cosmic rays and IMF in the vicinity of interplanetary shocks. *Adv. Space Res.* 2008, vol. 41, iss. 6, pp. 955–961. DOI: [10.1016/j.asr.2007.04.044](https://doi.org/10.1016/j.asr.2007.04.044).
- Hayakawa H., Ebihara Y., Mishev A., Koldobskiy S., Kusano K., Bechet S., Yashiro S., et al. The solar and geomagnetic storms in 2024 May: A flash data report. *Astrophys. J.* 2025, vol. 979, iss. 1, 26 p. DOI: [10.3847/1538-4357/ad9335](https://doi.org/10.3847/1538-4357/ad9335).
- Ievenko I.B. Effects of magnetospheric activity on the plasmasphere as inferred from observations of diffuse aurorae and SAR arcs. *Geomagnetism and Aeronomy*. 1999, vol. 39, iss. 6, pp. 697–703.
- Ievenko, I.B. SAR-arc observation during the overlap registration of an energetic plasma with a plasmopause aboard the Van Allen Probe. *J. Atmos. Solar-Terr. Phys.* 2020, vol. 209, 105386. DOI: [10.1016/j.jastp.2020.105386](https://doi.org/10.1016/j.jastp.2020.105386).
- Ievenko I.B., Alekseyev V.N. Effect of the substorm and storm on the SAR arc dynamics: A statistical analysis. *Geomagnetism and Aeronomy*. 2004, vol. 44, iss. 5, pp. 592–603.
- Ievenko I.B., Parnikov S.G. Ground-based and satellite observations of the SAR arc in the MLT evening sector at the beginning of the magnetic storm on March 17, 2015. *Geomagnetism and Aeronomy*. 2020, vol. 60, iss. 6, pp. 737–746. DOI: [10.1134/S0016793220050096](https://doi.org/10.1134/S0016793220050096).
- Kolesnik A.G., Golikov I.A. Three-dimensional model of the high-latitude F region taking into account the displacement between geographical and geomagnetic coordinates. *Geomagnetism and Aeronomy*. 1982, vol. 22, iss. 3, pp. 435–439.
- Korsakov A.A., Kozlov V.I., Karimov R.R. Sudden phase anomalies of VLF radio transmitters signals (11.9 kHz) of RSDN-20 system registered in Yakutsk during 2009–2017. *Proc. SPIE, 27th International Symposium on Atmospheric and Ocean Optics, Atmospheric Physics*. Moscow, Russian Federation, 2021, 119167X. DOI: [10.1117/12.2603367](https://doi.org/10.1117/12.2603367).

- Kozlov V.I., Starodubtsev S.A., Grigoryev V.G., Baishev D.G., Makarov G.A., Pavlov E.A., Karimov R.R., et al. Analysis of helio- and geophysical events in October–November 2021 from comprehensive observations of SHICRA SB RAS. *Sol.-Terr. Phys.* 2025, vol. 11, iss. 1, pp. 7–26. DOI: [10.12737/stp-111202502](https://doi.org/10.12737/stp-111202502).
- Kozyra J.U., Nagy A.F., Slater D.W. High-altitude energy source(s) for stable auroral red arcs. *Rev. Geophys.* 1997, vol. 35, iss. 2, pp. 155–190.
- Kumar A., Kumar S. Solar flare effects on D-region ionosphere using VLF measurements during low- and high-solar activity phases of solar cycle 24. *Earth, Planets and Space*. 2018, vol. 70, iss. 29, pp. 1–14. DOI: [10.1186/s40623-018-0794-8](https://doi.org/10.1186/s40623-018-0794-8).
- Lazzús J.A., Salfate I. Report on the effects of the May 2024 Mother's day geomagnetic storm observed from Chile. *J. Atmos. Solar-Terr. Phys.* 2024, vol. 261, 106304. DOI: [10.1016/j.jastp.2024.106304](https://doi.org/10.1016/j.jastp.2024.106304).
- Mizun Yu.G. *Polar Ionosphere*. Leningrad: Nauka Publ., 1980, 216 p.
- Moiseev A.V., Popov V.I., Starodubtsev S.A. Comparative analysis of the propagation of magnetic variations and equivalent current vortices of geomagnetic Pc5 pulsations along the meridian and azimuth. *Geomagnetism and Aeronomy*, 2024a, vol. 64, iss. 4, pp. 548–566. DOI: [10.31857/S0016794024040093](https://doi.org/10.31857/S0016794024040093).
- Moiseev A.V., Popov V.I., Starodubtsev S.A. Investigating azimuthal propagation of Ps5 geomagnetic pulsations and their equivalent current vortices from ground-based and satellite data. *Sol.-Terr. Phys.* 2024b, vol. 10, iss. 3, pp. 97–107. DOI: [10.12737/stp-103202412](https://doi.org/10.12737/stp-103202412).
- Petukhova A.S., Petukhov I.S., Petukhov S.I. Theory of the formation of Forbush decrease in a magnetic cloud: Dependence of Forbush decrease characteristics on magnetic cloud parameters. *Astrophys. J.* 2019, vol. 880, iss. 1, art. no. 17. DOI: [10.3847/1538-4357/ab2889](https://doi.org/10.3847/1538-4357/ab2889).
- Petukhova A.S., Petukhov I.S., Petukhov S.I. Forbush decrease characteristics in a magnetic cloud. *Space Weather*. 2020, vol. 18, iss. 12, art. no. e02616. DOI: [10.1029/2020SW002616](https://doi.org/10.1029/2020SW002616).
- Piersanti M., Oliveira D.M., D'Angelo G., Diego P., Napoletanj G., Zesta E. On the geoelectric field response to the SSC of the May 2024 super storm over Europe. *Space Weather*. 2025, vol. 23, e2024SW004191. DOI: [10.1029/2024SW004191](https://doi.org/10.1029/2024SW004191).
- Pilipenko V.A., Chernikov A.A., Soloviev A.A., Yagova N., Sakharov Y., Kudin D.V., Kostarev D., et al. Influence of space weather on the reliability of the transport system functioning at high latitudes. *Russian J. Earth Sciences*. 2023, vol. 23, ES2008. DOI: [10.2205/2023ES000824](https://doi.org/10.2205/2023ES000824).
- Ram T., Veenadhari S., Dimri B., Bulusu J., Bagiya M., Gurubaran S., Parihar N., et al. Super-intense geomagnetic storm on 10–11 May 2024: Possible mechanisms and impacts. *Space Weather*. 2024, vol. 22, e2024SW004126. DOI: [10.1029/2024SW004126](https://doi.org/10.1029/2024SW004126).
- Silber I., Price C. On the use of VLF narrowband measurements to study the lower ionosphere and the mesosphere–lower thermosphere. *Surveys in Geophysics*. 2017, vol. 38, iss. 2, pp. 407–441. DOI: [10.1007/s10712-016-9396-9](https://doi.org/10.1007/s10712-016-9396-9).
- Starodubtsev S.A., Transkii I.A., Verigin M.I., Kotova G.A. Intensity fluctuations of cosmic rays and of the interplanetary magnetic field in the region of interaction of solar-wind streams with different velocities. *Geomagnetism and Aeronomy*. 1996, vol. 36, pp. 241–245.
- Starodubtsev S.A., Zverev A.S., Gololobov P.Yu., Grigoryev V.G. Cosmic ray fluctuations and MHD waves in the solar wind. *Sol.-Terr. Phys.* 2023, vol. 9, iss. 2, pp. 73–80. DOI: [10.12737/stp-92202309](https://doi.org/10.12737/stp-92202309).
- Tavares M., Santiago M.A.M. What are traveling convection vortices? *Brazilian J. Physics*. 1999, vol. 29, iss. 3, pp. 524–528.
- Vorobjev V.G., Yagodkina O.I., Katkalov Yu.V. Auroral precipitation model and its application to ionospheric and magnetospheric studies. *J. Atmos. Solar-Terr. Phys.* 2013, vol. 102, pp. 157–171. DOI: [10.1016/j.jastp.2013.05.007](https://doi.org/10.1016/j.jastp.2013.05.007).
- Weimer D.R. A flexible, IMG dependent model of high-latitude electric potentials having “space weather” applications. *Geophys. Res. Lett.* 1996, vol. 23, no. 18, pp. 2549–2552.
- Wendt V., Schneider H., Banyś D., Hansen M., Clilverd M.A., Raita T. Why does the October effect not occur at night? *Geophys. Res. Lett.* 2024, vol. 51, iss. 7, pp. e2023GL107445. DOI: [10.1029/2023GL107445](https://doi.org/10.1029/2023GL107445).
- URL: <http://eng.sepc.ac.cn/> (accessed February 10, 2025).
- URL: <http://www.intermagnet.org> (accessed February 10, 2025).
- URL: <http://magdas2.serc.kyushu-u.ac.jp/station/index.html> (accessed February 10, 2025).
- URL: <http://www.isee.nagoya-u.ac.jp/dimr/PWING/en/> (accessed February 10, 2025).
- URL: <http://stjarnhimlen.se/comp/tutorial.html> (accessed February 10, 2025).
- URL: <ftp://ftp.swpc.noaa.gov/pub/lists/ace2/> (accessed February 10, 2025).
- URL: <ftp://ftp.swpc.noaa.gov/pub/lists/ace/> (accessed February 10, 2025).
- URL: <https://omniweb.gsfc.nasa.gov/ow.html> (accessed February 10, 2025).
- URL: <https://www.ysn.ru/~starodub/CosmicRayFluctuations/index.html> (accessed February 10, 2025).
- The 15th Russian-Chinese Workshop on Space Weather, September 9–13, 2024, Institute of Solar-Terrestrial Physics SB RAS, Irkutsk, Russia.*
- Original Russian version: Moiseev A.V., Gololobov A.Yu., Ievlenko I.B., Korsakov A.A., Petukhov I.S., Starodubtsev S.A., published in *Solnechno-zemnaya fizika*. 2025, vol. 11, no. 3, pp. 149–159. DOI: [10.12737/szf-113202516](https://doi.org/10.12737/szf-113202516). © 2025 INFRA-M Academic Publishing House (Nauchno-Izdatelskii Tsentr INFRA-M).
- Как цитировать эту статью:*
Moiseev A.V., Gololobov A.Yu., Ievlenko I.B., Korsakov A.A., Petukhov I.S., Starodubtsev S.A. Space weather research in Yakutia. *Sol.-Terr. Phys.* 2025, vol. 11, iss. 3, pp. 135–145. DOI: [10.12737/stp-113202516](https://doi.org/10.12737/stp-113202516).